Optics Communications 283 (2010) 4655–4661

Contents lists available at ScienceDirect

Optics Communications

journal homepage: www.elsevier.com/locate/optcom

# Ab-initio study of electronic and optical properties of InN in wurtzite and cubic phases

Tarun K. Maurya [a], S. Kumar [a,*], S. Auluck [b]

[a] Applied Physics Department, Institute of Engineering and Technology, M. J. P. Rohilkhand University, Bareilly- 243 006, India
[b] Department of Physics, Indian Institute of Technology, Kanpur-208 016, India

ARTICLE INFO

*Article history:*
Received 29 October 2009
Received in revised form 31 May 2010
Accepted 2 July 2010

*Keywords:*
FPLAPW
GGA
Electronic structure
Optical properties

ABSTRACT

We have performed systematic first principle calculations for the electronic and optical properties of a narrow band gap semiconductor InN in cubic and wurtzite phases by 'state-of-the-art' DFT calculations within generalized gradient approximation (GGA) and Engel–Vosko's corrected generalized gradient approximation (EVGGA) using full potential linear augmented plane wave (FPLAPW) method as implemented in WIEN2k code. The total energy for the wurtzite phase of InN was found to be smaller by 0.0184 Ry/molecule by cubic phase which confirms the greater stability of the wurtzite structure than the cubic one. Band structure, effective masses, density of states, valence charge densities, and dielectric functions are computed and presented in detail. The critical points are extracted out of calculated dielectric function, compared with available measured data and are explained in terms of transitions occurred in the band structure along different symmetry and antisymmetry lines. The valence band maxima and conduction band minima are strongly dominated by N-2p states and located at the Γ-symmetrical line which predicts its direct band gap nature in both phases.



## 1. Introduction

In the last few years no other class of material of semiconductors has attracted so much scientific and commercial attention like the group III-nitrides. The increasing interest is due to their extraordinary physical properties. The family of group III-nitrides, in particular, has been successfully used in the construction of blue light emitting diodes by Nakamura and co-workers [1,2]. As a consequence of the rapid improvement in both experimental and computational techniques, research on the physical properties of materials, especially group III-nitrides has seen much activity in recent years. Among the group III-nitrides, narrow band gap material InN has received much attention nowadays, but less studied in the past due to several problems encountered during the proper growth of high quality InN epitaxial layer such as low dissociation temperature (≈600 °C), extremely high equilibrium vapour pressure of nitrogen and large size differences between cation and anion [1] etc. The prospects of a narrow band gap ≈0.7 eV [3] generated much interest as it raised the possibility that the nitrides would be used to make optical devices which operated from the deep UV region to the near infrared (IR) region. The superior transport properties [4], large saturation and extremely high drift velocity of InN suggested its promising potential for the development of high speed or high frequency optoelectronic devices. It is now become easier to grow a good quality of crystalline material InN successfully by molecular beam epitaxy (MBE) and metal organic vapour phase epitaxy (MOVPE) etc. which further confirms its existence in the wurtzite and cubic phases. The most common growth direction for wurtzite InN is the [0001] direction known as *c*-axis. The *c*-axis is a polar direction which means that the crystal has an inherent electric field along this axis. The polarity arises due to lack of inversion symmetry in the wurtzite crystal which results in some charge separation along the *c*-axis. Davydov et al. [6], Wu et al. [7] and Matsuoka et al. [8] had grown a successfully good quality layer of crystalline wurtzite InN by the MBE and MOVPE technique respectively. Kurimoto et al. [9] and Aderhold et al. [10] had grown single crystalline *n*-InN on sapphire substrate by metal organic chemical vapour decomposition (MOCVD). The experimental results obtained from optical absorption, photoluminescence (PL) and photoluminescence excitation of InN gave unambiguous evidence that the fundamental band gap [6,7] is less than 1 eV. Shubina et al. [11] measured photoluminiscence of hexagonal InN films grown by MOCVD. Goldhahn et al. [3] measured the dielectric function of wurtzite InN in the energy range from 0.72 eV up to 9.5 eV by ellipsometric studies confirming the band gap of about 0.7 eV. Wu et al. [7] and Matsuoka et al. [8] confirmed that MBE and MOCVD grown wurtzite InN shows an evidence for a band gap near 0.7 eV. This value of band gap is much lower than the long term accepted band gap of about 1.9 eV by Tansley and Foley [5]. Optical measurements taken by Davydov et al. [6] for wurtzite InN revealed a strong photoluminescence in the range of 0.75 eV to 0.9 eV. First experimental results for dielectric function measurement of cubic InN taken by Goldhahn [12] up to photon energies of 10 eV revealed a band

* Corresponding author. Tel./fax: +91 581 2524232.
*E-mail address:* drsudhirkumar.in@gmail.com (S. Kumar).

0030-4018/$ – see front matter © 2010 Elsevier B.V. All rights reserved.
doi:10.1016/j.optcom.2010.07.011

gap of 0.595 eV. The zincblende (cubic) structure is of technological interest as it can be doped more easily than the wurtzite structure. Schörmann et al. [13] had grown cubic InN films on *c* GaN/3C-SiC hybride substrate by plasma assisted MBE at different growth temperature and estimated a band gap of 0.56 eV at room temperature.

As far as theoretical predictions are concerned regarding the electronic, structural and other properties, several authors [14–16,19–23] have reported results based on the density functional theory (DFT). Few calculations of wurtzite InN have been reported using different techniques. Mahboob et al. [17] had explained the origin of electron accumulation on wurtzite InN surfaces measurements as well as studied theoretically the energy band structure by ab-initio calculation using VASP code [18]. Furthmuller et al. [19] investigated the influence of quasi particle and the excitonic effect on band structure and optical spectra using VASP code [18]. Persson et al. [15] have presented the first principle calculations of the dielectric function of zincblende and wurtzite InN with quasi particle band gap correction. Usuda et al. have also presented first principle electronic band structure calculations of wurtzite InN within LDA and GW approximations [16]. Piper et al. [20] have measured valence band spectra and compared it with calculated valence band density of states (VB-DOS) using the VASP code [18]. Bechstedt et al. [21] reported optical absorption of narrow gap InN in terms of single particle band and, two particle coulomb interaction using VASP code [18]. Litimein et al. [22] have used APW + *lo* method to study the *d*-electron effect on electronic structure of zincblende and wurtzite InN.

Briki et al. [23] have used two different exchange correlations in non-relativistic and relativistic approach to explain the energy band gap with the FPLAPW method [24]. Rinke et al. [25,26] have calculated band gap and band parameters form quasi particle energy calculations of InN employing many body perturbation theory in the GW approximation. Band structure and effective mass calculations have been presented by Gorczyca et al. [27] by using the LMTO-ASA method. Zaoui et al. [28] had investigated the optical properties of hexagonal InN by using the all-electron LDA approach [24,29]. Cai et al. [30] have investigated the vibrational and electronic properties of amorphous InN using VASP code [18].

In spite of several reported results as discussed above, we are not aware of any systematic theoretical study which compares the calculated optical properties, particularly, the dielectric functions, origin of critical points (CPs) along with the possible band to band transitions for wurtzite and cubic InN. Hence, we thought it worthwhile to perform detailed calculations of electronic, and optical properties using full potential linearized augmented plane wave (FPLAPW) method.

In this paper, we mainly present the results of the FPLAPW based method which is used to reproduce the electronic band structure, projected density of states, charge densities, bulk modulus, effective masses with main emphasis on the frequency dependent dielectric functions and origin of critical points along with possible transitions that occurred along different symmetry lines as compared to available experimental findings for wurtzite and cubic InN. The paper is organized as follows; In Section 2, we discuss the method of calculations and computational details. Results and discussion for different properties are presented in Section 3. Section 4 summarises the results.

## 2. Computational details

The adopted DFT based computational approach for the present work is full potential linearized augmented plane wave (FPLAPW) method as implemented in WIEN2k code [24,29]. The Kohn and Sham equation have been treated within the generalized gradient approximation (GGA) and Engel–Vosko's corrected generalized gradient approximation (EVGGA) for the exchange correlation term [31]. A basis set is achieved by dividing the unit cell into non-overlapping atomic spheres (centered on the atomic sites) and an interstitial region. The applied basis set consists of 39,223 and 5211 plane waves in the interstitial region for cubic and wurtzite structure respectively. We have used optimized values of lattice constants, $a = 3.511$ Å and $c = 5.536$ Å for the wurtzite phase and 5.169 Å for the cubic phase of InN. A primitive cell of 2-atoms per unit cell for wurtzite and 8-atom supercell for cubic InN are taken as computational cell. In the wurtzite InN structure, atomic positions of In and N atoms are; In (0, 0, 0), (1/3, 2/3, 1/2); N (0, 0, 0), (1/3, 2/3, 1/2 + *u*) whereas the 8-atom cubic InN supercell was constructed by conventional 2-atom zincblende structure in which In and N have the positions; In (0, 0, 0); N (1/4, 1/4, 1/4). For the wurtzite structure the internal parameter *u* which is the relative displacement between In and N sublattices along the *c*-direction was fixed and equal to 0.375 and the *c*/*a* ratio at the value of 1.610. The atomic sphere radii are chosen 2.00 and 1.80 a.u. and kept constant throughout the calculations for In and N respectively in both phases. In the muffin-tin (MT) spheres, the *l*-expansion of non-spherical potential and charge density was carried out up to $l_{max} = 10$. In order to energy eigenvalue convergence, the basis function is expanded up to $R_{MT}K_{max} = 7.0$ (where $K_{max}$ is the maximum modulus for the consistency for the reciprocal lattice vector and $R_{MT}$ is the average radius of the MT-sphere). The Brillouin zone integrations were carried out using the tetrahedron method [32]. The total energies are calculated using 125 k-points in the irreducible Brillouin zone (IBZ). The self consistency was obtained using a dense mesh of 399 k-points in the IBZ. Since calculation of optical properties requires a more dense k-space matrix, we use 512 k-points for the calculation of the dielectric functions for wurtzite and cubic InN. The frequency dependent dielectric function can be calculated as

$$\varepsilon(\omega) = \varepsilon_1(\omega) + i\varepsilon_2(\omega) \tag{1}$$

For cubic structure, principal component of $\varepsilon_2(\omega)$ are equal i.e. $\varepsilon_2^{xx}(\omega) = \varepsilon_2^{yy}(\omega) = \varepsilon_2^{zz}(\omega)$ and can be calculated by standard expression which has been discussed in our previous paper [33–35].

Since wurtzite InN has hexagonal lattice, the frequency dependent optical properties are expected to be anisotropic. For hexagonal structures, the experiments are performed with electric vector **E** parallel or perpendicular to the *c*-axis. The corresponding imaginary parts of the dielectric function are $\varepsilon_2^{\parallel}(\omega)$ and $\varepsilon_2^{\perp}(\omega)$. Calculation of these dielectric functions involves the energy eigenvalues and electron wave functions which are natural outputs of the band structure calculations. We have performed calculations of the imaginary part of the frequency dependent interband dielectric function using the expressions [36]

$$\varepsilon_2^{\parallel}(\omega) = \frac{12}{m\omega^2}\int_{BZ}\sum_{nn'}\frac{|P^Z_{nn'}(k)|^2 dS_k}{|\nabla\omega_{nn'}(k)|}, \tag{2}$$

$$\varepsilon_2^{\perp}(\omega) = \frac{6}{m\omega^2}\int_{BZ}\sum_{nn'}\frac{[\,|P^X_{nn'}(k)|^2 + |P^Y_{nn'}(k)|^2\,]dS_k}{|\nabla\omega_{nn'}(k)|}. \tag{3}$$

The above expressions are written in atomic units with $e^2 = 1/m = 2$ and $\hbar = 1$, where $\omega$ is the photon energy and $P^X_{nn'}(k)$ is the X component of the dipole matrix elements between initial $|nk\rangle$ and final $|n'k\rangle$ states with their eigenvalues $E_n(k)$ and $E_{n'}(k)$, respectively. $\omega_{nn'}(k) = E_n(k) - E_{n'}(k)$, is the energy difference, and $S_k$ is a constant-energy surface defined as

$$S_k = \{k;\ \omega_{nn'}(k) = \omega.$$

## 3. Results and discussion

### 3.1. Structural parameters

We have optimized the lattice constants for both wurtzite and cubic InN. The calculated lattice constants in both phases, bulk

**Table 1**
Calculated GGA total energy $E_{tot}$ (in Ry/molecule), lattice constants (in Å), bulk modulus B (in GPa) and its first-pressure derivative, band gap (in eV).

| Parameters | wz InN | Exp. | Others | Cubic InN | Exp. | Others |
|---|---|---|---|---|---|---|
| $E_{tot}$ | −11,593.84288 | – | – | −11,593.82484 | – | – |
| $a$ | 3.511 | 3.540 | 3.49[b], 3.533[l] | 5.169 | 5.01±0.01[h] | 5.06[i], 5.00[j], 4.96[k], 4.98[l] |
| $c$ | 5.536 | 5.70 | 5.61[b], 5.693[l] | – | – | – |
| $B$ | 125.08 | 126,139[a] | 149[b] | 126.14 | 137[a] | 146[b], 121[i], 140[j], 141[k] |
| $B'$ | 5.0 | – | 4.38[b] | 6.03 | – | 4.38[b], 4.63[i], 4.38[j], 3.75[k] |
| $m_{\perp}^{*}$ | 0.051 | 0.050[c], 0.04[d] | 0.072[e], 0.10[f] | 0.053 | – | 0.054[l] |
| $m_{\parallel}^{*}$ | 0.050 | 0.050[c], 0.05[d] | 0.068[e], 0.10[f], 0.67[l] | – | – | – |
| $E_g$(GGA) | 0.26 | 0.70[g] | −0.179[b], 0.72[l] | 0.10 | 0.56[h] | 0.368[b], −0.561[i], −0.40[j], 0.59[k], 0.53[l], 0.60[m] |
| $E_g$(EVGGA) | 0.38 | 0.70[g] | 0.36[n] | 0.54 | 0.56[h] | 0.15[n] |

[a]Ref. [45], [b]Ref. [22], [c]Ref. [26], [d]Ref. [46], [e]Ref. [47], [f]Ref. [48], [g]Ref. [3], [h]Ref. [13], [i]Ref. [23], [j]Ref. [49], [k]Ref. [19], [l]Ref. [25], [m]Ref. [50], [n]Ref. [15].

modulus, and total energies are presented in Table 1 and compare well with the measured and available other theoretical calculations [15,19,22,23]. The wurtzite crystal structure is characterized by three parameters; the lattice constant $a$, the $c/a$ ratio, and the internal parameter $u$ which fixes the relative position of two hexagonal closed packed sublattices. Ideally, it is characterized by equal bond length, $c/a$ is $\sqrt{8/3}$ and $u$ is 3/8. Since $c/a$ is an independent parameter hence we allow the volume to relax to the one that gives the minimum total energy. Our calculations show that total energy for wurtzite structure of InN is smaller by 0.0184 Ry/molecule to cubic structure of InN. The small difference in total energy provides greater stability of wurtzite InN than the cubic one. When the $c/a$ ratio is optimized, we found a maximum deviation of 2.0% from the experimental value. Our calculated $c/a$ ratio is 1.577 in contrast to experimental value of 1.610.

## 4. Electronic properties

### 4.1. Band structure and projected density of states

The self consistent scalar relativistic electronic band structures for wurtzite and cubic InN along the symmetry lines are presented in Fig. 1. It is well known that the self consistent band structure within the density functional theory, usually underestimates the energy band gap [37,38]. This underestimation of the band gap is due to the fact that the exchange correlation have simple forms that are not sufficiently flexible to reproduce both the exchange correlation energy and its derivative. Engel and Vosko considered this shortcoming and constructed a new functional form of GGA [39] which is able to better reproduce the exchange potential at the expense of less agreement in exchange energy. On the other hand EVGGA, yields a better band splitting and some other properties which mainly depend on the accuracy of exchange correlation potential. However, in this method the quantities which depend on an accurate description of total energy such as equilibrium volumes and bulk modulus etc. are usually not in agreement with the experiments [37,39]. We have calculated the band structure of InN in both phases along the high symmetry lines in the Brillouin zone under GGA and EVGGA schemes.

The overall band structure behaviour calculated by these approximations is very similar except for the value of their band gap (see Table 1). The band structures calculated within EVGGA are presented in Fig. 1, where anionic and cationic states are expected to constitute the top of the valence band and the bottom of the conduction band. The valence band maximum and conduction band minimum can be seen at Γ-symmetry point which confirms its direct band gap nature in both phases. The magnitude of the band gap and the correct ordering of the valence bands at Γ can be noticed. It is known that cation-$d$ and anion-$p$ coupling reduces the band gaps in nitride compounds [40,41]. Also, the lower value of band gap is due to weaker overlapping of $s$, $p$-orbitals localized at the nearest neighbour atoms [42]. We have mentioned the contributions made by the anion and cation responsible for the formation of main bands in both phases. Accordingly, one can see the N-$2p$, In-$5p$ states form the upper valence band. Similar contributions by these states can be noticed for the formation of lowest and second lowest conduction bands. Our calculated band structures are in agreement with previous calculations [19,22,23,25].

Moving on projected density of states (PDOS), it is clear from PDOS as presented in Fig. 2 that the entire range of projected density of states is dominated by N-$2s$,$2p$ states in both phases. The PDOS can be divided in to four main groups. The first group i.e. lowest energy group

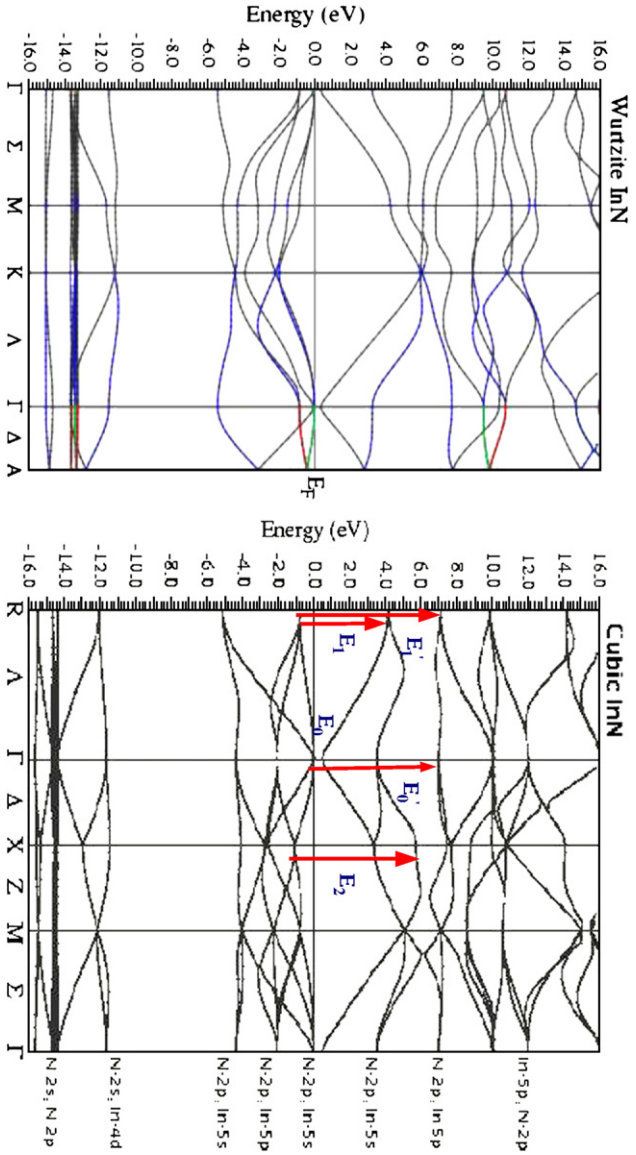


**Fig. 1.** Calculated band structures of wurtzite and cubic InN presented along different symmetry directions.

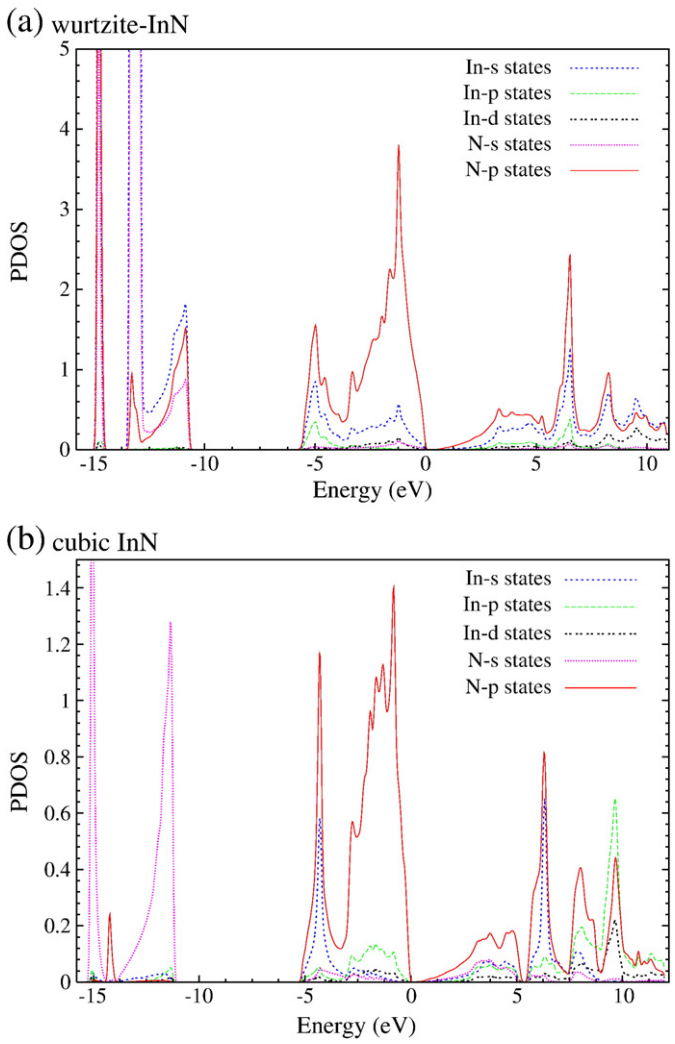


**Fig. 2.** Calculated projected density of states of wurtzite and cubic InN presented in (a) and (b) respectively.

(−15.0 eV to −11.5 eV) is mainly dominated by N-*2s* states in cubic InN whereas in this energy range a mixed hybridization of In-*5s*, N-*2s*,*2p* states can be seen for wurtzite InN. The second group between −5.0 eV to Fermi level is composed of N-*2p*, In-*5s* states with dominating features of N-*2p* states in both phases. The third group between Fermi level to +5.0 eV is composed of N-*2s*,*2p* and In-mph5s states. The strong hybridization of In-*5s*, 5*p* and N-*2p* states can be seen in the last group from +5.0 eV and above. However, the contribution of In-*4d* states near the top of the valence band and bottom of the conduction band is very small. Hence In-*4d* electronic states are seems to be localized and show almost no dispersion. Overall a strong hybridization is noticed between In-*5s*, N-*2s*,*2p* states above and below the Fermi level. Comparison of the calculated total density of states of wurtzite InN is presented in our previous calculations [43,44] with measured X-ray photoemission spectra [20] and other calculations [19,20,22,25] shows overall good qualitative agreement.

The first principle method is capable to derive an accurate charge density from the highly converged wave functions. The charge density can then be used to study the bonding nature of the solid. Hence, we have calculated the charge densities for wurtzite and cubic InN presented in Fig. 3. The similarity between wurtzite and cubic InN has been observed in the calculated band structures and PDOS as well. Total valence charge densities for both phases are displayed along the In-N bonds and in the [110] plane containing In and N atoms. In Fig. 3 the electronic charge distribution indicates that there is a strong ionic character for both structures and can be seen along In-N bonds. This similarity can basically be attributed to the local tetrahedral environment in the wurtzite and zincblende structures which causes the total charge density to be the same. The overall shape of the charge distribution i.e. positive contour plots around In and N suggests a highly ionic bonding nature and similar charge transfer from cation to anion.

## 5. Optical properties

The calculated real $\varepsilon_1(\omega)$ and imaginary part $\varepsilon_2(\omega)$ of the dielectric functions (DF) for wurtzite and cubic InN along with different critical points (CPs) are presented in Figs. 4 and 5 respectively. A Lorentzian broadening of 0.1 eV is used for the smoothness of the calculated spectra

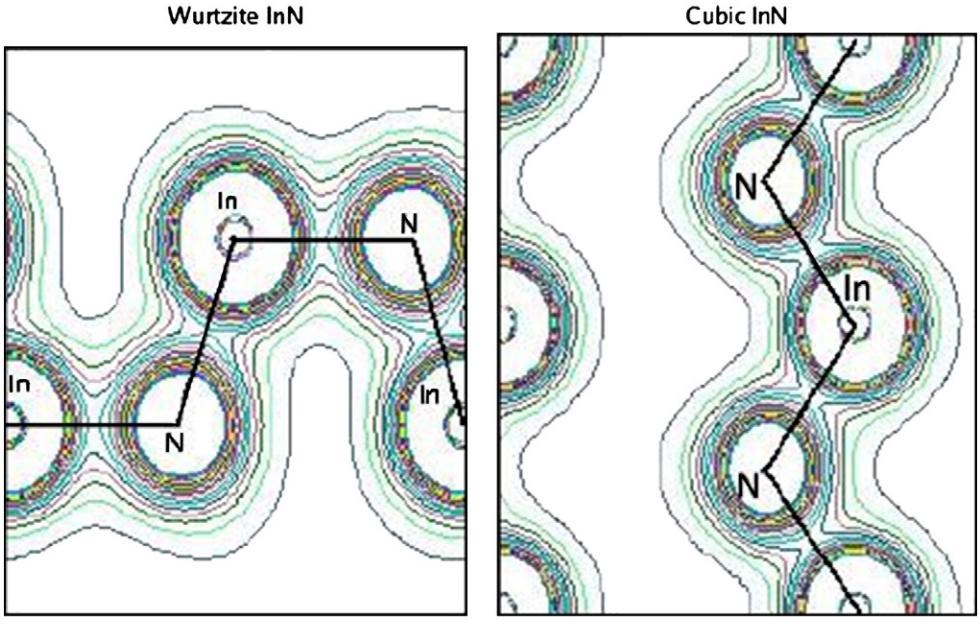


**Fig. 3.** Contour plots of valence charge densities of InN along [110] direction for wurtzite and cubic InN are presented. Units are $e/a.u^3$ and the contour step in 0.01 $e/a.u^3$.

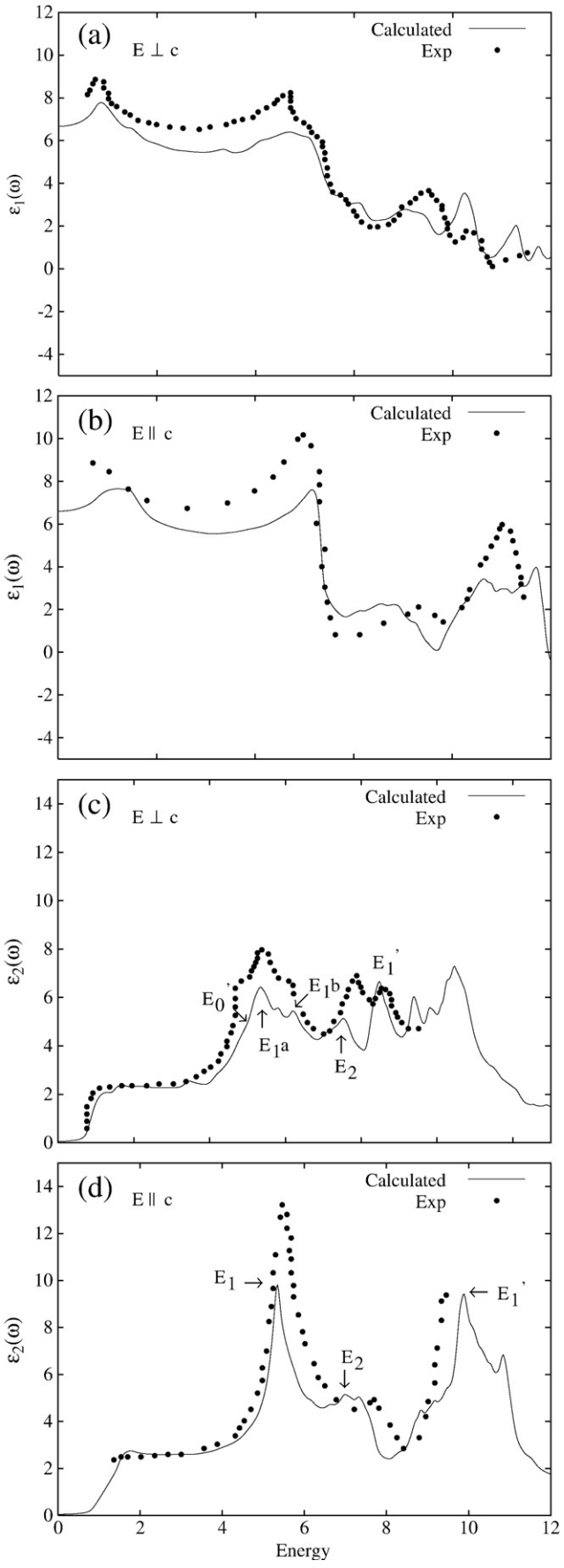


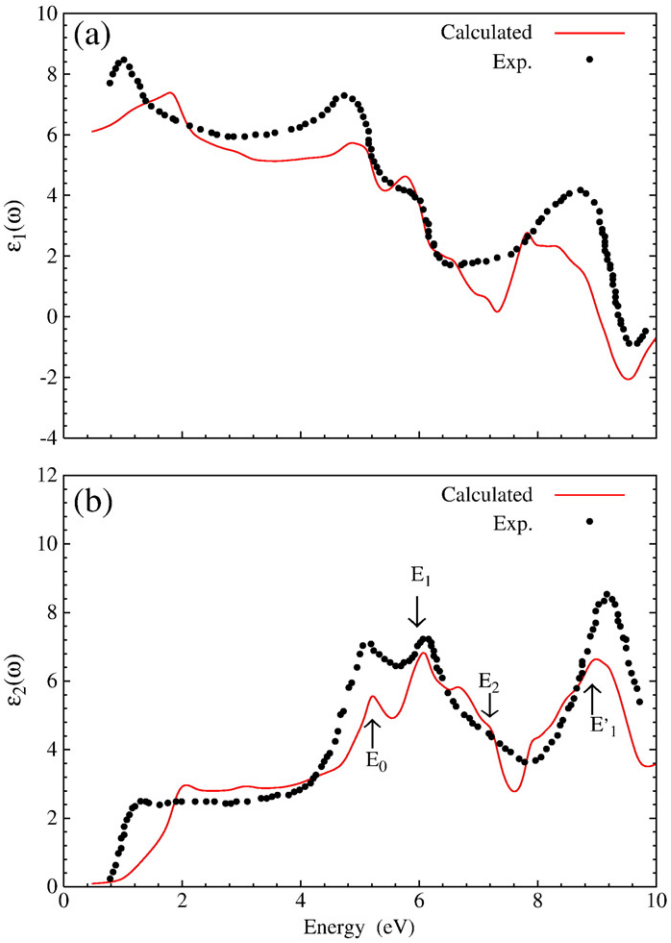


**Fig. 5.** Calculated dielectric functions (real and complex) for cubic InN presented in (a), (b) respectively along with measured data.

of dielectric function. For wurtzite InN, dielectric functions in two different polarizations i.e. $E \| c$ and $E \perp c$ are calculated. The positions of peaks observed in $\varepsilon_2(\omega)$ due to interband transitions in the wurtzite and cubic InN are presented in Table 2 for comparison. The $\varepsilon_2(\omega)$ of wurtzite InN can be seen with remarkable differences in Fig. 4(c) and (d). For the ordinary component we can identify absorption structures at 4.81, 5.76, 6.08, 7.88 and 8.14 eV while in the extraordinary component, we identify three main structures at 5.38, 6.98 and 9.83 eV up to 10.0 eV. These structures are in very good agreement with only available measured data [3,12] as presented in Table 2. The direct band gap of wurtzite InN is equal to 0.26 eV, therefore transitions start from 0.26 eV, as shown in Fig. 4(c) and (d) and attain a maxima at 5.76 eV and 5.38 eV. From Fig. 2(a) and (b), it is confirmed that the edge of the valence band maxima and conduction band minima of wurtzite and cubic InN have same type of hybridization. Therefore, the structure at 0.26 eV could be due to the transition from the occupied In-d and N-p states to the unoccupied N-p states. The predicted dielectric function for wurtzite InN shows a strong anisotropy i.e. extraordinary DF tensor component differ from ordinary DF tensor as presented in Fig. 4. The small peak in between the region 1.5 eV to 1.7 eV could be due to transitions from the In-*s* states to the N-*p* states. The sharp rise in $\varepsilon_2(\omega)$ at 5.38 eV is due to transitions from the In-*s*,*p* to the N-*p* states. The calculated $\varepsilon_1(\omega)$ for $E \| c$ and $E \perp c$ shows almost similar trends for wurtzite InN. The calculated DF tensor for cubic InN along with measured data [3,12] for real and complex part of the dielectric functions are presented in Fig. 5. For cubic

**Fig. 4.** Calculated dielectric functions (real and complex) for wurtzite structure along $E \| c$ and $E \perp c$ direction are presented in (a), (b), and (c), (d) respectively along with measured data.

**Table 2**
Calculated critical points (CPs) in $\varepsilon_2(\omega)$ for cubic and wurtzite InN (all in eV).

| CPs | wz $E\perp c$ | | | wz $E\parallel c$ | | | Cubic | |
|---|---|---|---|---|---|---|---|---|
| | Theory | Interband transition | Exp.[a, b] | Theory | Interband transition | Exp.[a, b] | Theory | Inerband transition |
| $E_0$ | 0.26 | $\left(\Gamma_6^v-\Gamma_1^c\right)$ | 0.7 | 0.26 | $(\Gamma_1^v-\Gamma_1^c)$ | 0.7 | 0.54 | $\left(\Gamma_{15}^v-\Gamma_1^c\right)$ |
| $E_0'$ | 4.81 | $\left(\Gamma_5^v-\Gamma_3^c\right)$ $\left(A_{5,6}^v-A_{5,6}^c\right)$ | 4.82 | – | $(\Gamma_6^v-\Gamma_6^c)$ $\left(A_{5,6}^v-A_{5,6}^c\right)$ | – | 4.84 | $\left(\Gamma_{15}^v-\Gamma_{15}^c\right)$ |
| $E_{1a}$ | 5.76 | $\left(\Gamma_5^v-\Gamma_3^c\right)$ | 5.38 | 5.38 | $(\Gamma_1^v-\Gamma_1^c)$ | 5.40 | 6.03 | $(R_3^v-R_1^c)$ |
| $E_{1b}$ | 6.08 | $(M_4^v-M_3^c)$ | 6.18 | – | – | – | – | |
| $E_2$ | 7.88 | $(K_3^v-K_2^c)$ | 7.94 | 6.98 | $(K_2^v-K_2^c)$ | 7.61 | 6.53 | $\left(X_5^v-X_1^c\right)$ |
| $E_1'$ | 8.14 | $\left(A_{5,6}^v-A_{1,3}^c\right)$ | 8.54 | 9.84 | $(\Gamma_3^v-\Gamma_6^c)$ | 8.54 | 8.84 | $(R_3^v-R_3^c)$ |

[a]Ref. [3], [b]Ref. [12].

InN one can see the main structures in $\varepsilon_2(\omega)$ at 5.13, 6.03, 6.53 and 8.84 eV. The structure at about 5.13 eV may be due to the transition from the In-3p, 3d states just below the Fermi level to the In-4s and N-2p states of the bottom of the conduction band. The peaks at 6.03 and 6.53 correspond to transitions from In-4s,3p of valence band to In-4s and N-2p states of the conduction band. The broad structure around 8.84 eV attributed to the mixed transition from In-4s, 3d and N-2p states of valence band to In-2p, 3d and N-2p states of the conduction band. Our calculated peaks were found to be shifted towards the lower energy because GGA underestimate the band gap. Hence we have shifted rigidly the calculated GGA based $\varepsilon_2(\omega)$ spectra by using scissor operator correction (SOC) by 0.52 eV and 0.70 eV for wurtzite and cubic phase respectively so as to match the onset of measured $\varepsilon_2(\omega)$. The overall calculated real and imaginary parts of the dielectric function in both phases are well in agreement with the experiment [3,12].

### 5.1. Critical point analysis

For both wurtzite and cubic InN we have identified main critical points (CPs) i.e. $E_0$, $E_0'$, $E_1$, $E_{1a}$, $E_{1b}$, $E_2$, and $E_1'$. These labels (CPs) for the characteristic absorption structures correspond in the isoelectronic sequence scheme to peaks observed in dielectric function spectra. We have presented the different transitions corresponding to different CPs for both wurtzite and cubic InN in Table 2. The CPs $E_0$ and $E_0'$ correspond to transition at Γ point. The CP $E_0$ which is also called as the absorption edge of the spectra arises mainly due to transition $\Gamma_6^v$–$\Gamma_1^c$ for $E\perp c$ and $\Gamma_1^v$–$\Gamma_1^c$ for $E\parallel c$ of wurtzite structure while for cubic structure it arises due to transition $\Gamma_{15}^v$–$\Gamma_1^c$. This CP also predicts the optical band gap for the material. We found a common band gap of magnitude 0.26 eV for wurtzite InN in two polarizations while 0.54 eV for cubic InN. The CP $E_0'$ is responsible for the mixed transition $\Gamma_5^v$–$\Gamma_3^c$ and $A_{5,6}^v$–$A_{5,6}^c$ when $E\perp c$ but when $E\perp c$ the corresponding transitions are $\Gamma_6^v$–$\Gamma_6^c$ and $A_{5,6}^v$–$A_{5,6}^c$. The location of main CP $E_1$ of the dielectric function can easily be traced in almost same range of energy for both wurtzite and cubic InN. This similarity of energy range for $E_1$ can be attributed to similar symmetry of zincblende (cubic) ±[111] directions to that of the corresponding wurtzite ±[0001] $c$-axis, therefore a direct correlation can be found between the CP $E_1$ of cubic InN with $E_1$ of the wurtzite InN. In the case when $E\perp c$, two sub peaks for $E_1$ can be seen in contrast to a single main peak as observed in cubic InN. The reason is as follows:

In general, the eight fold degeneracy of the corresponding cubic states is assumed as disturbed states in the hexagonal structure. Moreover, the Brillouin zone of the wurtzite structure has actually only one half of the volume of the zincblende (cubic) zone. In this double zone scheme the wurtzite state along $c$-direction can be obtained as disturbed zincblende (cubic) states along the [111] direction. As a result the corresponding $\Gamma_{15}(zb)$ states are treated as splited state in to $\Gamma_1$ and $\Gamma_5$ respectively. This leads to the splitting of $E_1$ into two smaller peaks as $E_1(a)$ and $E_1(b)$ which are clearly marked in the dielectric function spectra when $E\perp c$. This feature is also in agreement with the experimental evidences [12]. The CP $E_1$ arises mainly due to transitions $\Gamma_5^v$–$\Gamma_3^c$, $M_4^v$–$M_3^v$ when $E\perp c$ and due to $\Gamma_1^v$–$\Gamma_1^c$ when $E\parallel c$. The $\Gamma_5^v$–$\Gamma_3^c$ transition is only allowed for $E\perp c$ and corresponds to the folded L point (at present R-point in cubic structure) of zincblende (cubic) Brillouin zone. On the other hand for cubic structure it arises due to transition $R_{15}^v$–$R_{15}^c$. The interpretation of peak $E_2$ in wurtzite InN at about 7.0 eV is more complex. This structure does not energetically agree with the $E_2$ in the cubic dielectric function. The CP $E_2$ arises mainly due to transitions $K_3^v$–$K_2^c$ and $K_2^v$–$K_2^c$ for wurtzite structure when $E\perp c$ and $E\parallel c$ respectively while the corresponding peak $E_2$ for zincblende (cubic) InN is responsible due to transitions $X_5^v$–$X_1^c$. The last absorption structure $E_1$ can be seen between 8.0 eV to 10 eV in the two wurtzite dielectric components as well as in the cubic InN dielectric function. This absorption is associated in the wurtzite structure to different interband transitions including the $A_{5,6}^v$–$A_{1,3}^c$, $\Gamma_3^v$–$\Gamma_6^c$. All these transitions correlate with cubic $E_1$ at the R-point between $R_{15}^v$–$R_{15}^c$. The obtained critical point energies are well in agreement with the only available measured data [12].

## 6. Conclusions

We have discussed a comparative study of electronic, structural properties with main focus on optical transitions for wurtzite and cubic InN under GGA and EVGGA schemes. Our calculated band gaps, bulk modulus are in agreement with previous calculations. The calculated dielectric function for both phases shows good agreement with experimental data. We are able to get trends of $\varepsilon_2(\omega)$ that are in agreement with the experimental data. The CPs extracted from $\varepsilon_2(\omega)$ $E_0$, $E_0'$, $E_1$, $E_{1a}$, $E_{1b}$, $E_2$, and $E_1'$ are discussed in detail and show good agreement with the measured data.

## Acknowledgements

This work is supported by the Department of Science and Technology (DST), Council of Scientific and Industrial Research (CSIR) New Delhi. One of the authors (S. Kumar) are thankful to Prof. R. Goldhahn Technical University of Ilmenau, Germany for providing the measured data prior to publication.

## References

[1] S. Nakamura, The Blue Laser diode, Springer, Berlin, 1997.
[2] G. Fasol, Science 208 (1997) 1902.
[3] R. Goldhahn, A.T. Winzer, V. Cimalla, O. Ambacher, C. Cobet, W. Richter, N. Esser, J. Furthmüller, F. Bechstedt, H. Lu, W.J. Schaff, Superlattices Microstruct. 36 (2004) 591.
[4] A. Bhuiyan, A. Hashimoto, A. Yamamoto, J. Appl. Phys. 94 (2003) 2779.
[5] T.L. Tansely, C.P. Foley, J. Appl. Phys. 59 (1986) 3241.

[6] V. Yu Davydov, A.A. Klochikhin, R.P. Seisyan, V.V. Emtsev, S.V. Ivanov, F. Bechstedt, J. Furthmüller, J.H. Harima, A.V. Mudryyi, J. Aderhold, O. Semchinova, J. Graul, Phys. Stat. Sol. (b) 229 (2002) R1.
[7] J. Wu, W. Walukiewicz, K. JA Yu III, E. Haller, H. Lu, W. Schaff, Y. Saito, Y. Nanishi, Appl. Phys. Lett. 80 (2002) 3967.
[8] T. Matsuoka, H. Okamoto, M. Nakao, H. Harima, E. Kurimoto, Appl. Phys. Lett. 81 (2002) 1246.
[9] E. Kurimoto, H. Harimaw, A. Hashimoto, A. Yamanoto, Phys. Stat. Sol. (b) 228 (2001) 1.
[10] J. Aderhold, V. Davydov, F. Fedler, J. Crystal Growth 222 (2001) 2001.
[11] T.V. Shubina, S.V. Ivanov, V.N. Jmerik, D.D. Solnyshkov, V.A. Veshkin, P.S. Kop'ev, A. Vasson, J. Leymarie, A. Kavokin, H. Amano, K. Shimono, A. Kasic, B. Monemar, Phys. Rev. Lett. 92 (2004) 117407.
[12] R. Goldhahn, P. Schely, M. Roppischer, Ellipsometry of InN and Related Alloys, CRC Press 2007, Private Communications: http://www.bessy.de.
[13] J. Schormann, D.J. As, K. Lischka, P. Schley, R. Goldhahn, S.F. Li, W. Loffler, M. Hetterich, H. Kalt, Appl. Phys. Lett. 89 (2006) 261903.
[14] F. Bechstedt, Adv. Solid State Phys. 32 (1992) 161.
[15] C. Persson, R. Ahuja, A. Ferreira da Silva, B. Jhonsson, J. Phys. Condens. Matter 13 (2001) 8945.
[16] Manabu Usuda, Niriaki Hamada, Kenji Shiraishi, Atsushi Oshiyama, Jpn. J. Appl. Phys. 43 (2004) L407.
[17] I. Mahboob, T.D. Veal, L.F.J. Piper, C.F. McConville, Hai Lu, W.J. Schaff, J. Furthmuller, F. Bechstedt, Phys. Rev. B 69 (2004) 201307R.
[18] G. Kresse, J. Furthmuller, Comput. Mater. Sci. 6 (1996) 15.
[19] J. Furthmuller, P.H. Hahn, F. Fuchs, F. Bechstedt, Phys. Rev. B 72 (2005) 205106.
[20] L.F.J. Piper, T.D. Veal, P.H. Jefferson, C.F. Mc-Conville, F. Fuchs, J. Furthmüller, F. Bechstedt, Hai Lu, W.J. Schaff, Phys. Rev. B 72 (2005) 245319.
[21] F. Bechstedt, J. Furthmuller, P.H. Hahn, F. Fuchs, J. Crystal Growth 288 (2006) 14043.
[22] F. Litimein, B. Bouhafs, P. Ruterna, Phys. Stat. Sol. (a) 203 (2006) 35.
[23] M. Briki, A. Zaoui, F. Boutaiba, M. Ferhat, Appl. Phys. Lett. 91 (2007) 182105.
[24] P. Blaha 2001 Computer code WIEN2k Vienna University of Technology which was published by P. Blaha updated Unix/Linux version of the original copyrighted WIEN code K. Schwartz 1990 Comput. Phys. Commun. 59 339.
[25] P. Rinke, M. Scheffler, A. Qteish, M. Winkelnkemper, D. Bimberg, J. Neugerbauer, Appl. Phys. Lett. 89 (2006) 161919.
[26] P. Rinke, M. Scheffler, A. Qteish, M. Winkelnkemper, D. Bimberg, J. Neugerbauer, Phys. Rev. B 77 (2008) 075202.
[27] I. Gorczyca, L. Dmowski, J. Plesiewicz, T. Suski, N.E. Christensen, A. Svane, C.S. Gallinat, G. Koblmueller, J.S. Speck, Phys. Stat. Sol. b 245 (No.5) (2008) 887.
[28] A. Zaoui, M. Ferhat, Solid State Commun. 149 (2009) 329.
[29] http://www.wien2k.at.
[30] B. Cai, D.A. Drabold, Phys. Rev. B 79 (2009) 195204.
[31] J.P. Perdew, Phys. Rev. B 45 (1992) 13244.
[32] O. Jepson, Solid State Commun. 9 (1971) 1763.
[33] S. Kumar, Tarun K. Maurya, S. Auluck, J. Phys. Condens. Matter 20 (2008) 75205.
[34] S. Kumar, Tarun K. Maurya, S. Auluck, Jpn. J. Appl. Phys. 47 (No. 7) (2008) 5417.
[35] S. Kumar, Tarun K. Maurya, S. Auluck, J. Alloys Compd. 480 (2009) 417.
[36] S. Sangeeta, S. Auluck, M.A. Khan, Pramana J. Phys. 54 (2000) 431.
[37] P. Dufek, P. Blaha, K. Schwarz, Phys. Rev. B 50 (1994) 7279.
[38] F. El Hassan, H. Akbarzadeh, Comput. Mater. Sci. 53 (2006) 423.
[39] E. Engel, S.H. Vosko, Phys. Rev. B 47 (1993) 13164.
[40] V. Fiorentini, M. Methfessel, M. Scheffler, Phys. Rev. B 47 (1993) 13353.
[41] S.H. Wei, Phys. Rev. B 69 (1996) 2719.
[42] U. Grossner, J. Furthmuller, F. Bechstedt, Phys. Rev. B 58 (1998) 1722.
[43] Tarun K. Maurya, S. Kumar, S. Auluck, Conf. Proceedings NSU-XV, India, 2006, p. 184.
[44] Tarun K. Maurya, Ph.D Thesis (2008) M. J. P. Rohilkhand University, Bareilly-India.
[45] M. Uneo, M. Yoshida, A. Onodera, O. Shimomura, K. Takemura, Phys. Rev. B. 49 (1994) 14.
[46] A.T. Hofmann, T. Chavdarov, V. Darakchieva, H. Lu, W.J. Schaff, M. Schubert, Phys. Stat. Solidi C 3 (2006) 1854.
[47] D. Fritsch, H. Schmidt, M. Grundmann, Phys. Rev. B 69 (2004) 165204.
[48] D.J. Dugdle, S. Brand, R.A. Abram, Phys. Rev. B 61 (2000) 12933.
[49] C. Stampfl, C.G. van de Walle, Phys. Rev. B 59 (1999) 5521.
[50] A. Qteish, Al-Sharif, M. Fuchs, M. Scheffler, S. Boeck, J. Neugebauer, Phys. Rev. B 72 (2005) 155317.